Forward-cone-imaging OCT needle probe

Jigang Wu, Michael Conry, Chunhui Gu, Fei Wang, Zahid Yaqoob, et al.

Jigang Wu, Michael Conry, Chunhui Gu, Fei Wang, Zahid Yaqoob, Changhuei Yang, "Forward-cone-imaging OCT needle probe," Proc. SPIE 6079, Coherence Domain Optical Methods and Optical Coherence Tomography in Biomedicine X, 60791J (20 February 2006); doi: 10.1117/12.646554

SPIE.

Event: SPIE BiOS, 2006, San Jose, California, United States

Forward-cone-imaging OCT needle probe

Jigang Wu*, Michael Conry, Chunhui Gu, Fei Wang, Zahid Yaqoob and Changhuei Yang

Biophotonics Laboratory, Department of Electrical Engineering
California Institute of Technology, Pasadena, California, 91125

ABSTRACT

We propose a novel forward-imaging OCT needle probe. The probe is based on the use of two angled GRIN lenses that can freely rotate with respect to each other. The probe is capable of scanning a forward cone volume ahead of the probe tip. Different scanning modes, such as the conventional OCT B-scan mode, spiral mode and starburst B-scan mode, can be obtained by adjusting the angular scan velocities of the two GRIN lenses. We develop a prototype probe and demonstrate its capability to acquire OCT images. In this paper we give the characteristics of the prototype probe and display images of different part of tadpole acquired by the probe. The longitudinal resolution, lateral resolution and the signal-to-noise ratio of the system are 10 μm, 10 μm and 93 dB, respectively.

Keywords: Optical Coherence Tomography, Endoscopic probe, Forward-imaging.

1. INTRODUCTION

The invention of several kinds of endoscope probes for optical coherence tomography (OCT) have greatly extended the application range of this high-resolution biomedical imaging technique[1-5]. Most probe implementations can be divided into two groups according to their scanning mode, i.e., side scanning[1-3] and forward scanning[4, 5]. For the side scanning probe, probe miniaturization is a relatively simple task as the actual scan actuators for the probes can generally be located far from the probe tips. The smallest reported side scanning probe[2] has an outer diameter of 0.4 mm. By virtue of their small size, side-imaging OCT probes have been used to image saphenous vein[1], muscle[2] and colon[3], etc. In comparison, forward-imaging probes are generally more complicated in design. Further, the scan actuation schemes that have thus far been reported[4, 5], generally require the location of the actuators at or very near to probe tips. Unsurprisingly, forward-imaging OCT probes that have been reported are relatively large in probe diameter. The typical forward scanning probes are of much larger size, e.g., 2.4 mm reported in ref. 5. One of the important advantages of the forward scanning probe over the side scanning one is that it can be used to implement needle guidance as the acquired forward image can indicate the location of the needle. Image-based needle guidance is very useful in all types of needle biopsy procedures, e.g., lung[6], breast core biopsy[7]. Another important application area for image guidance is in anesthesiology procedures, where image guidance can dramatically reduce the risk of nerve bundle perforation by the needle[8]. Therefore, the research pursuit of a narrower (e.g., 2 mm or smaller diameter) forward-imaging OCT probe design with a wide field of view is an especially worthy one.

In this paper, we present a new design for a forward-imaging OCT needle probe – the Paired Angle Rotation Scanning OCT (PARS-OCT) probe. This probe design utilizes a pair of angle-cut rotating GRIN lenses to deflect and scan the OCT probe beam across the forward region ahead of the probe tip. In this design, the scan actuation system may be located away from the probe tip, much like in the case of a side-imaging OCT probe[1], enabling easy miniaturization of the actual probe. Further, this probe design can achieve a large forward scan arc length to probe diameter ratio. This parameter is especially relevant for clinical probe considerations, as a clinician will desire as wide a scan range as possible with the smallest possible probe size. Actually the use of small GRIN lens or gradient-index fiber as a probe has been reported by several other groups, although they are not using the GRIN lens to scan the laser beam[9, 10].

2. PRINCIPLES

The operating principle of the PARS-OCT probe is as follows. The PARS-OCT probe channels the input OCT probe light from a single mode fiber through the first GRIN lens [see Fig. 1(a) and (b)]. The light beam exits from the

* jigang@caltech.edu; phone 1 626 395 4711

Coherence Domain Optical Methods and Optical Coherence Tomography in Biomedicine X
edited by Valery V. Tuchin, Joseph A. Izatt, James G. Fujimoto, Proc. of SPIE Vol. 6079
60791J, (2006) · 1605-7422/06/$15 · doi: 10.1117/12.646554

other face of the GRIN lens which is cut at an angle ψ. The beam then enters the second GRIN lens through an identically angle-cut face of the GRIN lens. Finally, the beam exits the second GRIN lens and focuses at a point ahead of the probe. The exact focal point is determined by the pitch of the two GRIN lenses. Amongst other good choices, an appropriate choice will be to have a slightly longer than ¼ pitch GRIN lens for the first and a shorter than ¼ pitch GRIN lens for the second; this choice results in a weakly focused beam between the two GRIN lenses and a tightly focused exit beam with desired working distance. For completeness, we shall define the orientations of the two GRIN lenses by angles ζ_1 and ζ_2, which are defined as the angles between the projections of vectors $\hat{r}_1$ and $\hat{r}_2$, respectively, in the image plane and the x-axis [see Fig. 1(a)]. We shall define the direction of the output light beam by its polar angle θ that it makes with the z-axis and its azimuthal angle φ; an angle of θ = 0 implies that the exit beam propagates along the z-axis.

A fan sweep of the output beam in xz-plane [shown vertical in Fig. 1(d)] can be performed by simply rotating the two GRIN lenses in opposite directions at the same angular speed from the starting position where the two GRIN lenses are oriented such that $\zeta_1 = \zeta_2 = 0$. This scan pattern can be understood by taking a closer look at the output beam orientation when $\zeta_1 = \zeta_2 = 0$ [see Fig. 1(a)]. In this case, the exit beam from the first GRIN lens is deflected in the xz-plane such that φ = 0. Notice that the second GRIN lens with $\zeta_2 = 0$ further bends the beam (keeping φ = 0). In Fig. 1(d), it is shown as downward deflection. When we start to rotate the two GRIN lenses by an equal and opposite amount ($\zeta_1 = -\zeta_2 > 0$), the downward deflection of the exit beam from the first GRIN lens will lessen and the beam will lean to the left if we view the probe head on. The shifting of the beam to the left will be compensated by the second GRIN lens which conveys an equal but opposite shift to the beam; the downward deflection contribution of the beam by the second GRIN lens will lessen as well. The net effect is a smaller downward deflection of the beam and little or no horizontal shifting. Continued rotations of the GRIN lenses will eventually result in the GRIN lenses orientation of $\zeta_1 = 90^\circ$ and $\zeta_2 = -90^\circ$. In this configuration [see Fig. 1(b)], the two GRIN lenses compensate for each other's deflection of the beam and result in an output beam that is undeflected. Further rotation of the GRIN lenses will then deflect the beam upwards. A complete 180º rotation of the GRIN lens will therefore result in a vertical sweep of the output beam from its down position to its up position – a fan sweep or an effective OCT B-scan.

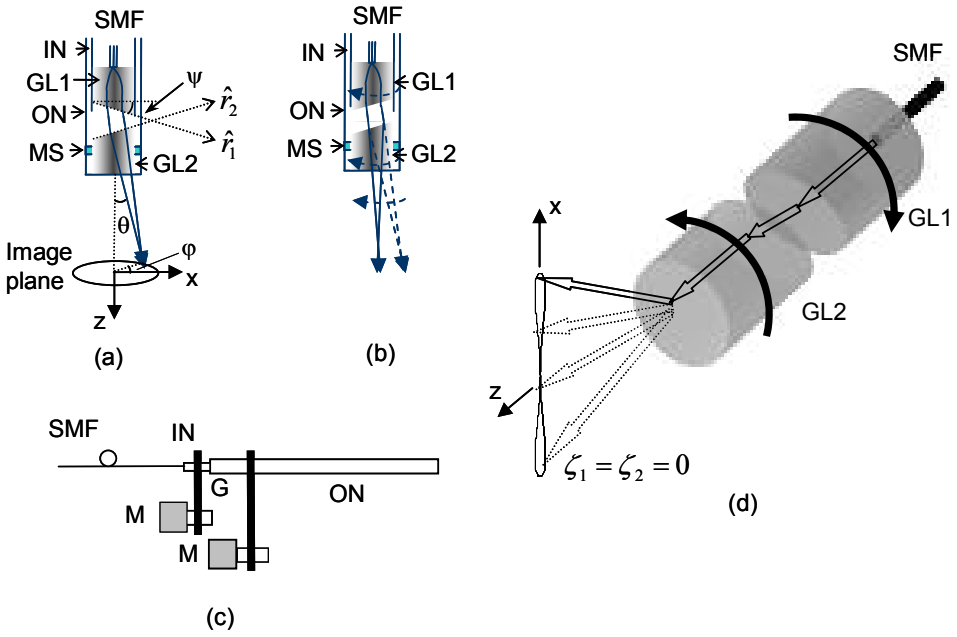

Fig. 1. Schematic of the forward-cone-imaging needle probe. (a) The case when there is an angle between the two angled surfaces of the GRIN lenses; the exit laser beam is tilted; (b) The case when the two angled surfaces of the GRIN lenses are parallel; the exit laser beam is undeviated; (c) PARS-OCT probe setup; (d) Profile of PARS-OCT B-scan mode. SMF: single-mode fiber; GL1: GRIN lens 1; GL2: GRIN lens 2; IN: inner needle; ON: outer needle; MS: metal sleeve; M: motor; G: gear.

The angular velocities of the DC motors can be controlled to perform different kinds of lateral scanning other than the conventional B scan shown above. For example, when both needles rotate in the same speed and in the same direction (in this case, θ remains the same while φ is changing), the focal spot will scan in a circular fashion. When both GRIN lenses rotate in the same direction with slightly different angular velocity (in this case, θ changes slowly while φ changes quickly), the focal spot will trace out a spiral. Finally, when both GRIN lens rotate in opposite direction with a slightly different speed (in this case, θ changes quickly while φ changes slowly), we can get a starburst scan pattern. The cases of spiral scanning and starburst scanning are shown in Fig. 2. In combination with the depth scanning capability of OCT, the last two scan mode will enable us to perform tomographic imaging of the forward cone volume of the probe.

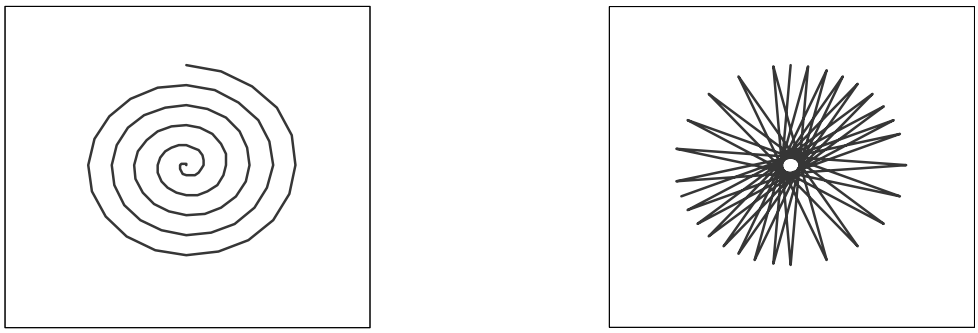

(a) (b)

Fig. 2. Scanning mode of the needle probe. (a) spiral scanning, when both needles rotate in slightly different speed and in the same direction; (b) starburst scanning, when both needles rotate in slightly different speed but in the opposite direction.

Because the refractive angle of the beam is changing during the rotation of the needles, the output power of the probe depends on the orientation of the needle. We measure the output power as the orientation of the needle changes for one of our prototype probes, as shown in Fig. 3. We can see from the data that the maximum variation is about 3 dB, which is acceptable for imaging.

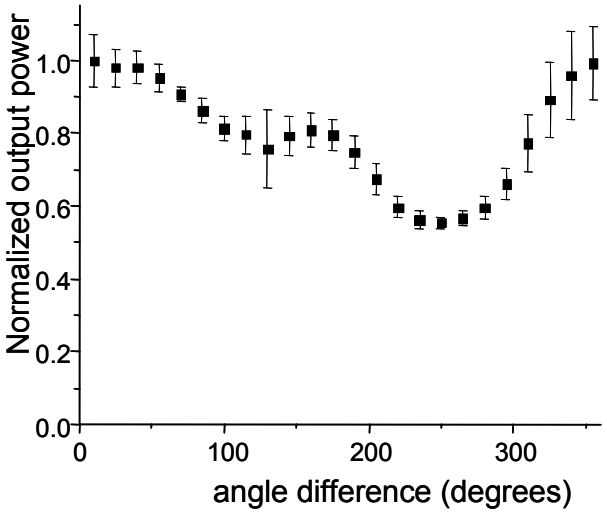

Fig. 3. The variation of the output power as the orientation of the needles changes.

There are three major advantages associated with this probe design. First, by attaching the GRIN lenses to separate concentric needle shafts, we can actuate the GRIN lenses rotations by simply turning the needle shafts. This can be done with actuators that are located far from the probe tip. Second, this probe design can more fully use the effective optical channel area of the probe than any of the other reported probe design. In an ideal probe, the exiting probe beam should completely occupy the output area of the probe; such a system will have the highest possible emission and collection numerical aperture. However, given the need to scan the output beam, this ratio of output beam area to the optical channel cross-section is much smaller than unity for all reported probe design. The PARS-OCT probe design can achieve a ratio of 0.8% for the parameters reported here (probe beam diameter defined by the FWHM of the beam intensity), and a ratio of 62.5% if the GRIN lenses used are swapped for a pair of diameter 112 μm, assuming the same GRIN material. In other reported forward-imaging OCT probe designs, the achievement of such a goal is hindered by the scan mechanism[4,5]. Finally, this probe design allows us to obtain a complete volumetric scan of the forward region. There are several ways to acquire such a volumetric scan. One simple way is to acquire a series of B-scans through the scan scheme described above and incrementally change the starting GRIN lenses' orientation between each scan.

3. EXPERIMENT

Based on this probe design, we fabricated a prototype PARS-OCT needle probe and provided a proof-of-principle demonstration of the PARS-OCT capability. The prototype consists of an inner needle (18XTW-gauge) and an outer needle (16TW-gauge) that are cut from standard hypodermic tubings (Poppers&Sons Inc.) and attached to a pair of angled GRIN lenses. The overall probe diameter is 1.65 mm. Both GRIN lenses (1 mm in diameter) are angle cut and polished at an angle ψ of 22º and suitable length. The measured working distance is 1.4 mm (from the exit face of the probe, when the exit light is straight) and the focused exit beam has a measured focal spot size of ~10.3 μm. When the exit light is tilted, the working distance will be slightly shorter (~1.27 mm) and the focal spot size will be slightly larger (~12.5 μm). Two DC motors attached to the proximal end of the probe provide the rotation actuation. Waterproofing the probe for surgical work can be done through numerous approaches. We evaluated the use of dental epoxy as a way to seal the probe and it proved to be sufficient – immersion in water of a treated probe did not change its performance.

The relationship between θ, ζ_1, and ζ_2 defies a simple analytical expression. Matlab simulation of the probe trajectory during B-scans [see Fig. 3(a)] shows a consistent up and down sweep trajectory with acceptable deviation (the ratio of the maximum angle deviation to the maximum sweep angle is 1.2%).

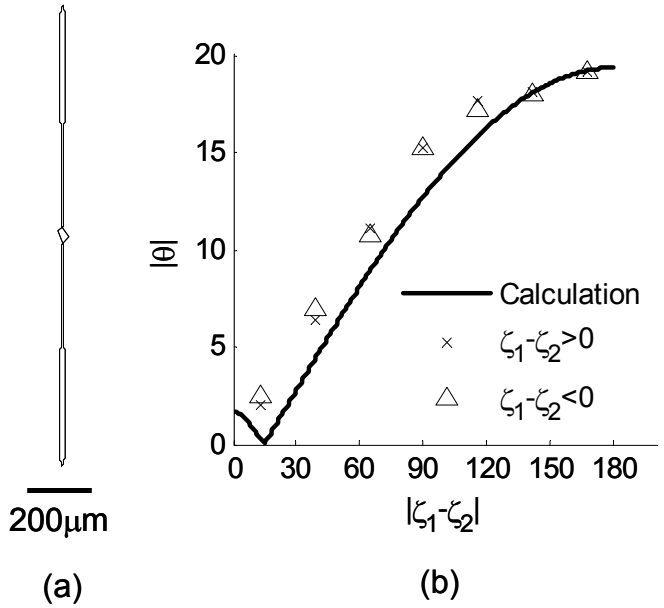

Fig. 3. (a) The calculated B-scan mode profile as projected in the focal plane of the exit beam. (b) Calculated and measured exit beam polar angle, $|\theta|$, versus the difference between the orientation angles of the two GRIN lenses, $|\zeta_1-\zeta_2|$.

To get a simplified expression of θ, we assume that the beam is collimated by the first GRIN lens, and then focused by the second GRIN lens. After the first GRIN lens, the angle between the collimated beam and the axis is (α−ψ), where $\alpha = \sin^{-1}(n\sin\psi)$. The ABCD matrix of the second GRIN lens can be written as, if we disregard the angled surface,

$$\begin{bmatrix} \cos(Z\sqrt{A}) & \frac{1}{N_0\sqrt{A}}\sin(Z\sqrt{A}) \\ -N_0\sqrt{A}\sin(Z\sqrt{A}) & \cos(Z\sqrt{A}) \end{bmatrix}$$

where N_0 and $\sqrt{A}$ are the on-axis refractive index and the index gradient constant of the GRIN lens, respectively. Z is the length of the second GRIN lens. To count in the angled surface, we first calculate the angle between the beam and the axis right after the refraction on the angled surface of the second GRIN lens, θ_1, and then calculate the equivalent incident beam angle for unpolished surface. By equivalent, we mean when the light is incident in this angle, we will get the same θ_1 after refraction on the unpolished GRIN surface.

Assuming (α−ψ) is small and the beam is paraxial, the expression of the θ as a function of ζ_1, ζ_2, can be derived as:

$$\theta = -N_0\sqrt{A}\sin(Z\sqrt{A})\cdot d\tan(\psi)(\alpha-\psi) + N_0\cos(Z\sqrt{A})\cdot\theta_1 \qquad (1)$$

where

$$\theta_1 = \sqrt{(1-\frac{1}{N_0})^2\sin^2\psi + 2(\frac{1}{N_0}-\frac{1}{N_0{}^2})(\alpha-\psi)\sin\psi\cos(\xi_1-\xi_2) + (\frac{\alpha-\psi}{N_0})^2} \qquad (2)$$

and $N_0\theta_1$ is the equivalent incident angle. We experimentally verify the agreement of the performance of the prototype probe to this simple formula by experimentally measuring |θ| versus $|\zeta_1-\zeta_2|$. The cases for $\zeta_1-\zeta_2>0$ and $\zeta_1-\zeta_2<0$, both shown in Fig. 3(b), indicate very good agreement between theory and experiment.

We next employed the PARS-OCT prototype probe to image a stage 54 Xenopus Laevis tadpole, which was euthanized before the experiment. The OCT engine employed in this experiment is based on a swept laser source with center wavelength 1300 nm, bandwidth 70 nm, power 2.5 mW, sweep rate 250 Hz and a theoretical SNR of around 125 dB. Dual balanced scheme is used to suppress excess noise[11].The system setup is shown in Fig. 4. The measured SNR of the PARS-OCT probe system is ~93 dB, the drop of SNR is due to the coupling loss within the probe and the beat noise caused by the interference between reference beam and internal reflections within the probe. The photograph of the probe and the tadpole is shown in Fig. 5.

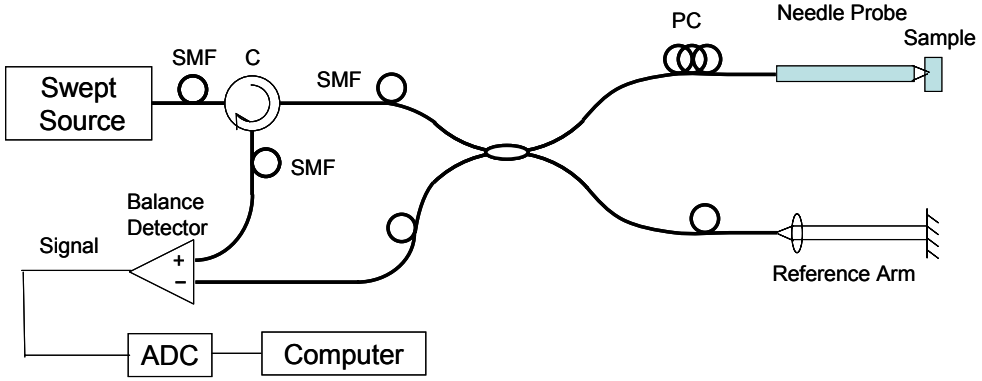

Fig. 4. Swept source OCT system setup. SMF, single-mode fiber; C, circulator; PC, polarization controller; ADC, analog-to-digital converter.

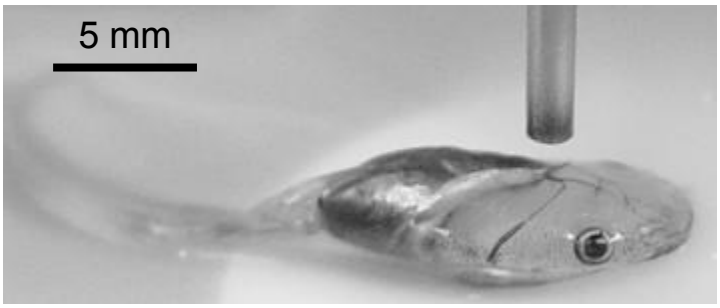

Fig. 5. The photograph of the needle probe and the tadpole.

In the demonstration, we rotated the two needles with equal and opposite speed and acquired OCT B-scan images from the specimen. Fig. 6 shows an OCT image of the tadpole heart. The image is shown in a fan plot according to the scan pattern of the probe. We can see the pericardium and the heart in the figure.

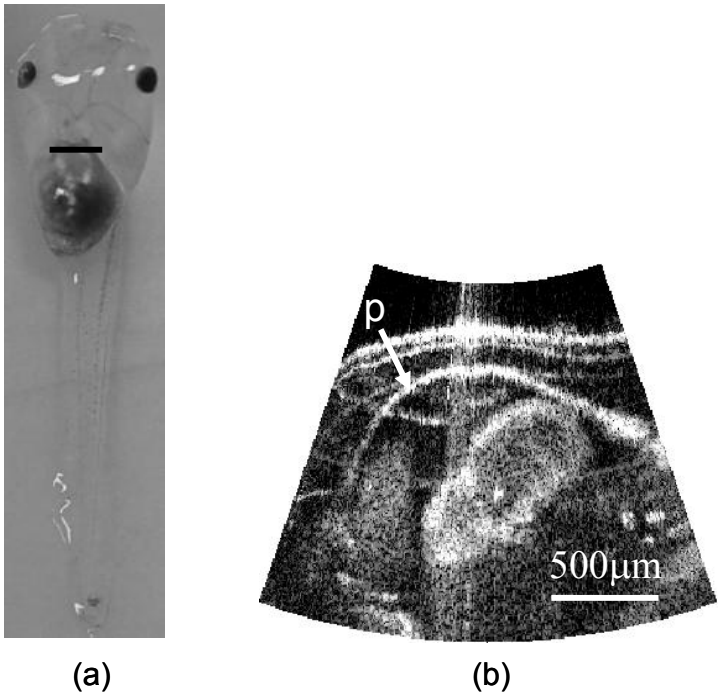

Fig. 6. (a) The photograph of the tadpole and the location where image is acquired. (b) The OCT image of a tadpole heart. The pixel number is 320 (lateral) × 250 (axial). p, pericardium.

By changing the initial position of the needles, we can do B-scan in different direction. To demonstrate this, we take OCT images of the tadpole gill structure in perpendicular directions, as shown in Fig. 7. We rotate both needles by 90 degree when acquiring the perpendicular image. The gill pockets can be clearly discerned in the images. By taking consecutive OCT B-scans in this way, we should be able to construct 3-D images of the object. The potential problem of this way of construction 3D image is that the paraxial region is over-sampled compared to the peripheral region. The spiral scanning mode might be a better approach when volumetric scanning is implemented.

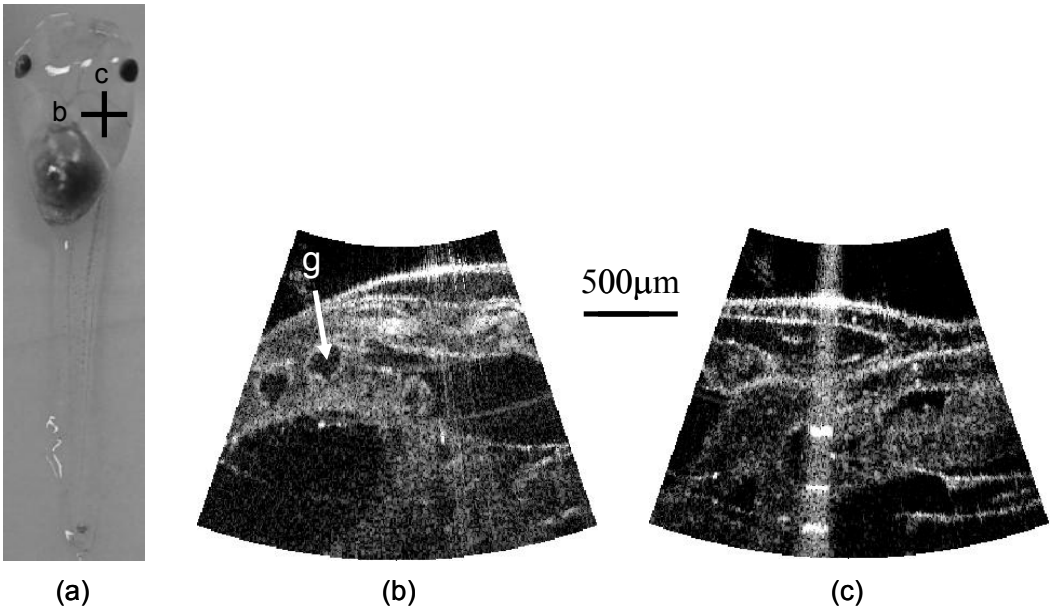

Fig. 7. (a) The photograph of the tadpole and the locations where images are acquired. (b)(c), The OCT images of the tadpole gill structure. The pixel number is 320 (lateral) × 250 (axial). g, gill pocket.

4. CONCLUSION

In summary, we have demonstrated a forward-cone-imaging OCT needle probe with a 1.65 mm outer diameter that can be used to acquire 3-D OCT images. Furthermore, the probe supports different scanning modes which can be used in different applications. The principle of the needle probe is straightforward and easy to implement. Since the GRIN lenses and the needles used in our design are commercially available and easy to miniaturize, smaller needle probe can be made. Also, we can attain a higher imaging speed by increasing the rate of rotation of the motors and the A-scan rate, the latter is already demonstrated in literatures both in time domain[12] and Fourier domain[13] OCT system. The probe can be potentially used in needle biopsy to provide high-resolution tomographic images of the targets forward of the probe.

5. ACKNOWLEDGEMENT

We thank Xin Heng for helpful discussions. This project is supported by funding from NIH: 5R21EB004602-02.

REFERENCES

1. G. J. Tearney, S. A. Boppart, B. E. Bouma, M. E. Brezinski, N. J. Weissman, J. F. Southern, and J. G. Fujimoto, "Scanning single-mode fiber catheter-endoscope for optical coherence tomography", Opt. Lett. **21**, 543-545 (1996)
2. Xingde Li, Christian Chudoba, Tony Ko, Costas Pitris, and James G. Fujimoto, "Imaging needle for optical coherence tomography", Opt. Lett. **25**, 1520-1522 (2000)
3. P. R. Herz, Y. Chen, A. D. Aguirre, K. Schneider, P. Hsiung, J. G. Fujimoto, K. Madden, J. Schmitt, J. Goodnow, and C. Petersen, "Micromotor endoscope catheter for in vivo, ultrahigh-resolution optical coherence tomography", Opt. Lett. **29**, 2261-2263 (2004)
4. Tuqiang Xie, Huikai Xie, Gary K. Fedder, and Yingtian Pan, "Endoscopic optical coherence tomography with a modified microelectromechanical systems mirror for detection of bladder cancers", Appl. Opt. **42**, 6422-6426 (2003)
5. Xiumei Liu, Michael J. Cobb, Yuchuan Chen, Michael B. Kimmey and Xingde Li, "Rapid-scanning forward-imaging miniature endoscope for real-time optical coherence tomography", Opt. Lett. **29**, 1763-1765 (2004)

6. Stephen Lam, Calum MacAulay, Jean C. leRiche, Branko Palcic, "Detection and localization of early lung cancer by fluorescence bronchoscopy", Cancer **89**, 2468-2473 (2000)
7. Tari A. King and George M. Fuhrman, "Image-guided breast biopsy", Seminars in Surgical Oncology **20**, 197-205 (2001).
8. Carl P. C. Chen, Simon F. T. Tang, Tsz-Ching Hsu, Wen-Chung Tsai, Hung-Pin Liu, Max J. L. Chen, Elaine Date, and Henry L. Lew, "Ultrasound guidance in caudal epidural needle placement", Anesthesiology **101**, 181-184 (2004)
9. William A. Reed, Man F. Yan, and Mark J. Schnitzer, "Gradient-index fiber-optic microprobes for minimally invasive in vivo low-coherence interferometry", Opt. Lett. **27**, 1794-1796 (2002)
10. Juergen C. Jung and Mark J. Schnitzer, "Multiphoton endoscopy", Opt. Lett. **28**, 902-904 (2003)
11. Michael A. Choma, Marinko V. Sarunic, Changhuei Yang, and Joseph A. Izatt, "Sensitivity advantage of swept source and Fourier domain optical coherence tomography", Opt. Express **11**, 2183-2189 (2003)
12. Andrew M. Rollins, Manish D. Kulkarni, Siavash Yazdanfar, Rujchai Ung-arunyawee and Joseph A. Izatt, "In vivo video rate optical coherence tomography", Opt. Express **3**, 219-229 (1998)
13. Maciej Wojtkowski, Vivek J. Srinivasan, Tony H. Ko, James G. Fujimoto, Andrzei Kowalczyk, and Jay S. Duker, "Ultrahigh-resolution, high-speed, Fourier domain optical coherence tomography and methods for dispersion compensation", Opt. Express **12**, 2404-2422 (2004)